

Seasonal and Interannual Variations in the Velocity Field of the South China Sea

CHAU-RON WU¹, PING-TUNG SHAW¹ and SHENN-YU CHAO²

¹*Department of Marine, Earth and Atmospheric Sciences, North Carolina State University, P.O. Box 8208, Raleigh, NC 27695, U.S.A.*

²*Horn Point Laboratory, University of Maryland Center for Environmental Studies, P.O. Box 775, Cambridge, MD 21613, U.S.A.*

(Received 12 March 1998; in revised form 6 July 1998; accepted 10 July 1998)

A three-dimensional numerical model is used to simulate sea level and velocity variations in the South China Sea for 1992–1995. The model is driven by daily wind and daily sea surface temperature fields derived from the NCEP/NCAR 40-year reanalysis project. The four-year model outputs are analyzed using time-domain Empirical Orthogonal Functions (EOF). Spatial and temporal variations of the first two modes from the simulation compare favorably with those derived from satellite altimetry. Mode 1, which is associated with a southern gyre, shows symmetric seasonal reversal. Mode 2, which contributes to a northern gyre, is responsible for the asymmetric seasonal and interannual variations. In winter, the southern and northern cyclonic gyres combine into a strong basin-wide cyclonic gyre. In summer, a cyclonic northern gyre and an anticyclonic southern gyre form a dipole with a jet leaving the coast of Vietnam. Interannual variations are particularly noticeable during El Niño. The winter gyre is generally weakened and confined to the southern basin, and the summer dipole structure does not form. Vertical motions weaken accordingly with the basin-wide circulation. Variations of the wind stress curl in the first two EOF modes coincide with those of the model-derived sea level and horizontal velocities. The mode 1 wind stress curl, significant in the southern basin, coincides with the reversal of the southern gyre. The mode 2 curl, large in the central basin, is responsible for the asymmetry in the winter and summer gyres. Lack of the mode 2 contribution during El Niño events weakens the circulation. The agreement indicates that changes in the wind stress curl contribute to the seasonal and interannual variations in the South China Sea.

Keywords:

- Seasonal variation,
- interannual variation,
- ocean current,
- South China Sea.

1. Introduction

The South China Sea, bordered by the Asian continent, Borneo, Palawan, Luzon and Taiwan, is the largest marginal sea in the Southeast Asian waters (Fig. 1). A string of islands on the east side of the basin separates the sea from the Pacific with three openings. The Luzon Strait is the widest and deepest with a sill depth of more than 2000 m, allowing inflow and outflow of deep waters (Nitani, 1972). The other two on the northern and southern ends of Palawan are narrow, and the exchange with the Sulu Sea is less important (Wyrski, 1961). The basin is elongated in the northeast-southwest direction. The wide Asian continental shelf, including the Gulf of Tonkin, is in the north with depths less than 100 m. The Gulf of Thailand and Sunda Shelf border the southern boundary of the sea with depths ranging from 50 m to 100 m. Depths of the central and eastern basin are between 1000 m and 5000 m.

Circulation in the South China Sea is driven by the East Asian monsoons, northeasterly in winter and southwesterly in summer. On a seasonal time scale, the surface circulation is cyclonic in winter and anticyclonic in summer. Both gyres intensify along the western boundary of the basin. The western boundary current off Vietnam, southward in winter and northward in summer, is asymmetric. In winter, the southward boundary current follows the western boundary throughout, but the northward boundary jet in summer separates from the coast at central Vietnam (Wyrski, 1961; Shaw and Chao, 1994). Upwelling in the South China Sea is persistent but localized. Two major upwelling areas are identified from observations. Off the coast of Vietnam, upwelling is manifested by a drop of more than 1°C in sea surface temperature in June and July (Wyrski, 1961; Levitus, 1984) and has been verified in model simulation (Chao, *et al.*, 1996a). Off northwest Luzon, subsurface upwelling in

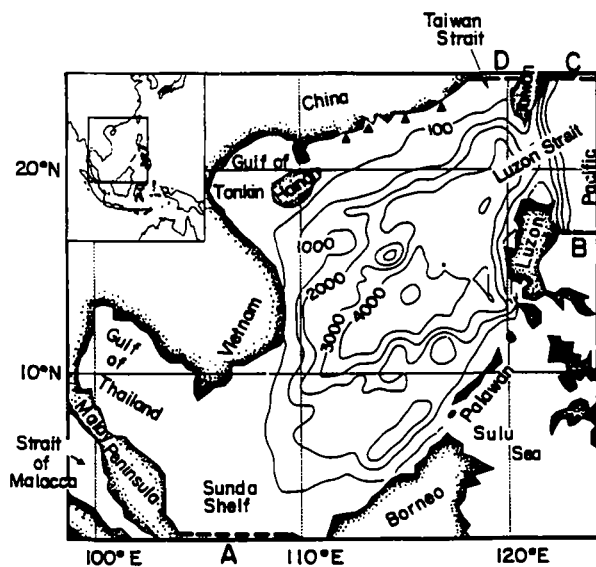


Fig. 1. Map of the South China Sea with the 100, 1000, 2000, 3000 and 4000 m isobaths shown. The small insert in the upper left gives the geographical location of the basin.

winter has been observed and attributed to the basin-wide gyre circulation (Shaw *et al.*, 1996).

Beyond the seasonal time scale, circulation of the South China Sea demonstrates interannual variations related to El Niño. From model simulation of the 1982–1983 El Niño episode, Chao *et al.* (1996b) showed that upwelling is weakened during El Niño because of a weaker basin-wide circulation under a weaker East Asian monsoon. Using TOPEX/POSEIDON altimeter sea level data from late 1992 to mid-1995, Shaw *et al.* (1997, manuscript submitted to *Oceanographica Acta*, hereafter SCF) confirmed the presence of a weaker circulation pattern during warm events. They also established the relevance of the wind stress curl to the sea level variation. The success of identifying variations in the altimeter data motivated us to study the variation in the velocity field and its relation to the sea surface variation further. Establishing the relationship between subsurface currents and sea level variation will help elucidate the subsurface processes, e.g. upwelling, in the basin, paving the way for future model-data assimilation.

With the Southern Oscillation Index remaining negative from 1990 to 1995, this five-year period has been identified as the longest El Niño on record since 1882 (Trenberth and Hoar, 1996). Using sea surface temperature anomalies averaged over 5°S–5°N and 150°W–90°W as a measure of El Niño intensities, Goddard and Graham (1997) identified three warm events with no intervening cold events during the first half of the 1990s. In this study, the model of Shaw and Chao (1994) is used to simulate daily sea level and velocity fields during the period from January 1, 1992 to December 31, 1995. The simulated sea level and velocity

fields are described using time-domain Empirical Orthogonal Functions (EOF) to facilitate comparison with concurrent TOPEX/POSEIDON altimeter data. EOF modes associated with the wind stress curl are also calculated to examine the driving mechanisms of the South China Sea circulation.

2. Model Description and EOF Analysis

The model of Shaw and Chao (1994) is a generalization of the Bryan-Cox code to accommodate for a free sea surface. It solves the three-dimensional equations of momentum, continuity, temperature, and salinity. Boussinesq and hydrostatic approximations are used. The integration domain is from 2°N to 24°N and from 99°E to 124°E. The horizontal resolution is 0.4°. The model contains 21 vertical layers. Open boundaries, marked by (A, B, C, D) in Fig. 1, are at the Taiwan Strait, the Sunda Shelf, and east of the Luzon Strait as in the previous study. At the open boundaries, radiation conditions are used except that depth-integrated transports are fixed to Wyrki's (1961) bimonthly estimates. For inflow, waters entering the basin are given the temperature and salinity as in Levitus' (1982) climatological atlas. A detailed description of the model has been given in Shaw and Chao (1994).

The model is initialized by the January temperature and salinity fields of Levitus (1982) and is under climatological forcing for two years as in Shaw and Chao (1994). After this spin-up period, the daily wind field and the daily sea surface temperatures from NCEP/NCAR 40-year reanalysis project (Kalnay *et al.*, 1996) are applied for four years beginning on January 1, 1992. The daily wind forcing in the present study reveals more details of the circulation in the basin than the monthly forcing used in previous modeling studies. Daily wind stresses, interpolated from a 2.5° resolution to the 0.4° model resolution, are prescribed at the beginning of each day. Time series of simulated daily sea level heights and velocities at 50 m depth at each grid point are smoothed and sampled every 10 days for EOF analysis. The 50 m depth is chosen because currents at this depth are not contaminated by strong Ekman flow and are representative of the surface circulation in the South China Sea (Shaw and Chao, 1994).

Utility of EOF analysis condenses information in the four-dimensional data derived from the model. The procedure of EOF analysis is as follows. Let Z be an n by m matrix consisting of m time series in column vectors of length n . These time series are real for a scalar quantity, such as sea level. For the velocity field, a complex time series $U + iV$ is formed from the eastward velocity U and the northward velocity V . The associated covariance matrix is $S = ZZ'$, where prime represents complex conjugate transpose. The eigenvalue problem is $Se = e\Lambda$, where e and Λ contain eigenvectors and eigenvalues, respectively. Each column of e , representing the eigenvector of one mode, describes time dependence and is normalized to a unit length. The spatial

dependence is given by the row vectors in $e'Z$. Since normalization is made for the column vectors in e , the relative importance of different modes is reflected in the plots of the spatial distribution.

3. Spatial and Temporal Variations of Sea Level Modes

EOF decomposition of sea level yields two dominant modes, explaining 88% and 8% of the variance, respectively. The next mode contributes 2% of the total variance. The study of SCF showed that variations associated with climatology and warm events are mainly contributed by the first two modes. Therefore, only modes 1 and 2 are presented

below. Figure 2 shows the spatial distribution of sea level associated with these two modes. Mode 1 demonstrates large amplitude oscillations centered at 8°N, 112°E in waters deeper than 1000 m in the southern basin. On the western shelves, oscillations are out of phase with the deep water variations; the extreme sea level is in the Gulf of Thailand. Sea level gradients southeast of Vietnam indicate the presence of a boundary current. Mode 2 is mainly contributed by oscillations centered at 14°N, 113°E in the deep basin and is out of phase with weak oscillations along the perimeter.

Temporal variations of sea level in each mode can be obtained by multiplying the modal amplitude (Fig. 2) by the coefficient shown in Fig. 3. Sea level variations associated with mode 1 reveal annual oscillations with extreme positive values in August and extreme negative values in December–January. On the western shelves, mode 1 sea level is low in August and high in December–January, showing the rise and fall of sea level driven by the monsoon winds in a rectangular basin (Csanady, 1982). In the deep waters of the southern basin, sea level is high in August and low in December. The sign changes in sea level gradients southeast of Vietnam show reversal of the coastal jet; northward in summer and southward in winter. Similarity in magnitude of the mode 1 coefficient in winter and summer indicates a nearly symmetric reversal of the southern gyre off Sunda Shelf. Mode 2 coefficient has extreme positive values around

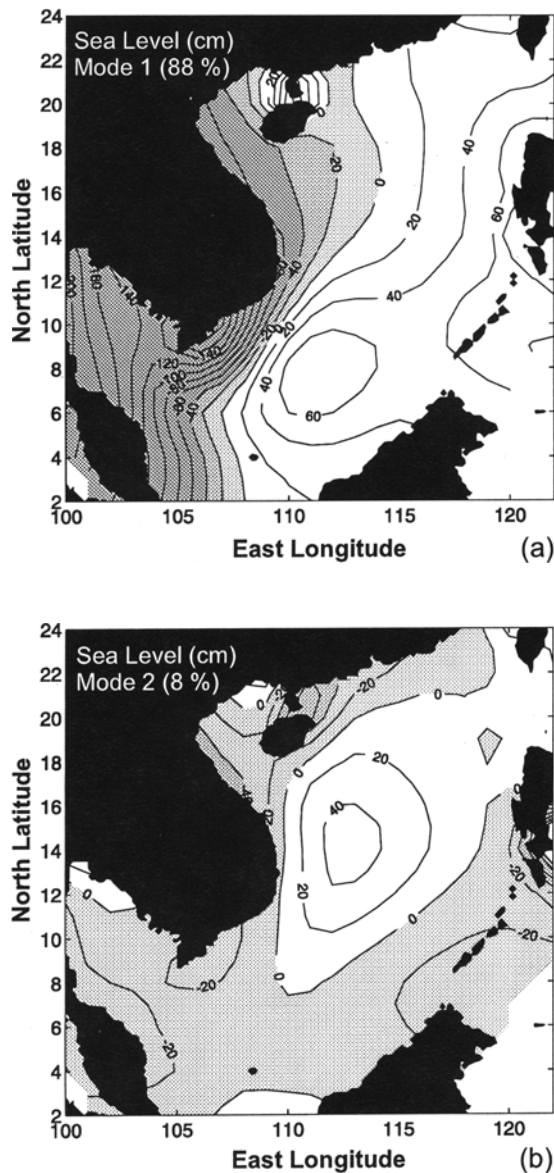


Fig. 2. Spatial structure of the first two sea level modes. Contour intervals are 20 cm, and negative contours are shaded.

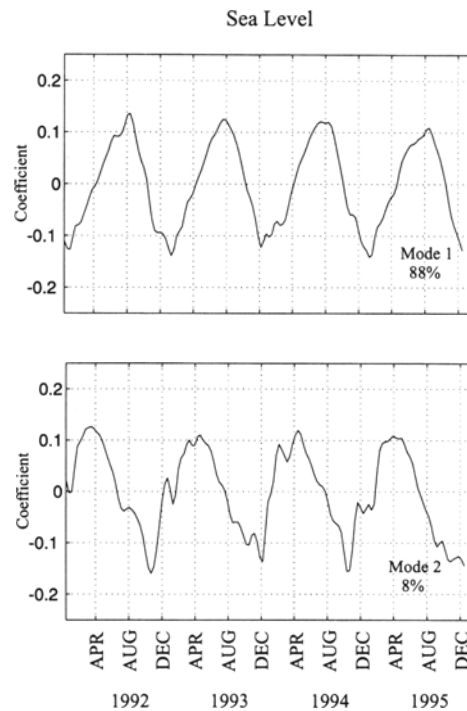


Fig. 3. Temporal variations of the first two sea level modes. Monthly marks are at the 15th day of each month.

April and extreme negative values in either October or December. In these months, the mode 1 coefficient is generally small, and the local maximum off central Vietnam in Fig. 2(b) dominates: high in April and low in October.

Year-to-year variations are present in the mode 2 coefficient (Fig. 3(b)). The coefficient generally decreases rapidly after April, becomes negative by August, and reaches extreme negative values thereafter. In 1993 and 1995, the mode 2 coefficient remains negative through the end of December. The negative coefficient produces a low off Vietnam in addition to the mode 1 low off the Sunda Shelf.

In these years, a strong low with two local maxima off Vietnam and Sunda Shelf spans the entire deep basin. In 1992 and 1994, the coefficient is large and negative in October, producing a low in sea level off Vietnam. This low disappears in December, when the mode 2 coefficient is nearly zero. Replacement of a Vietnam low by a Sunda low to the south from October to December is clearly shown in both satellite altimeter data in SCF and raw outputs of the present model. The coefficients of modes 1 and 2 are generally of opposite signs in summer and contribute to a different sea level pattern. In August, a negative mode 2 coefficient produces a low off central Vietnam. This low

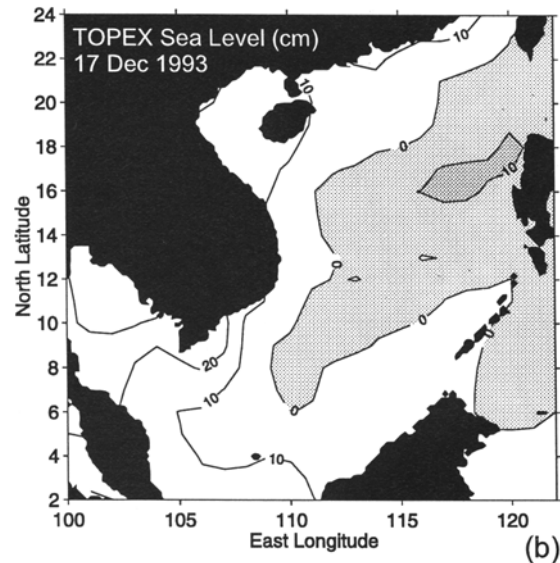
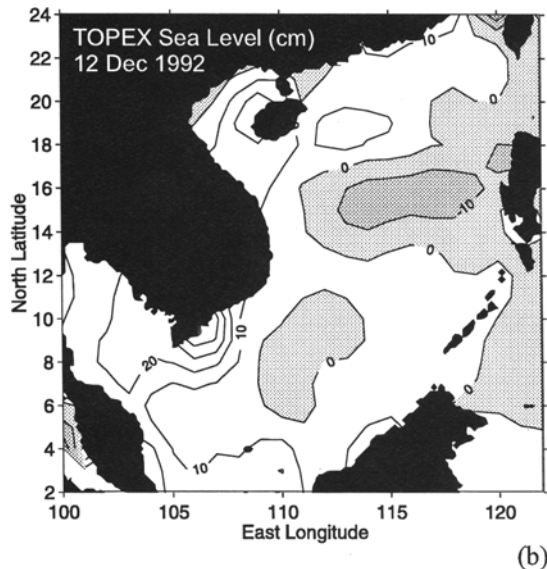
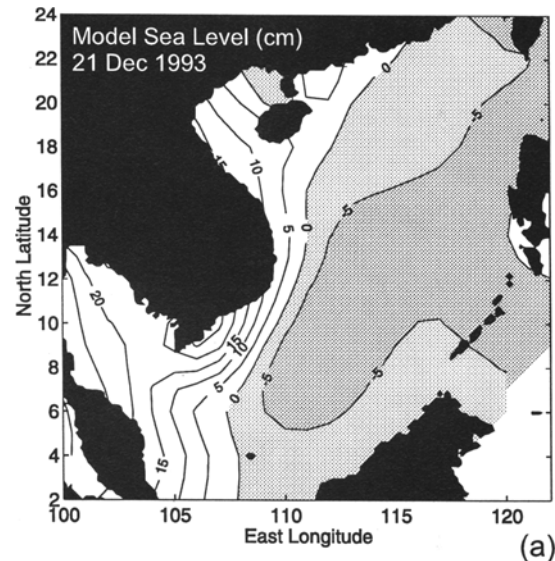
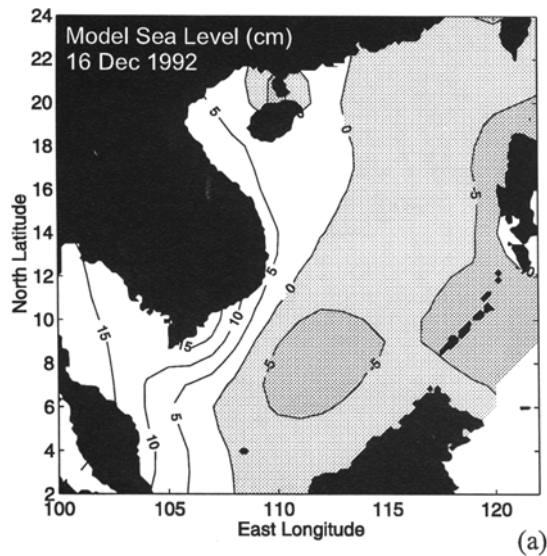


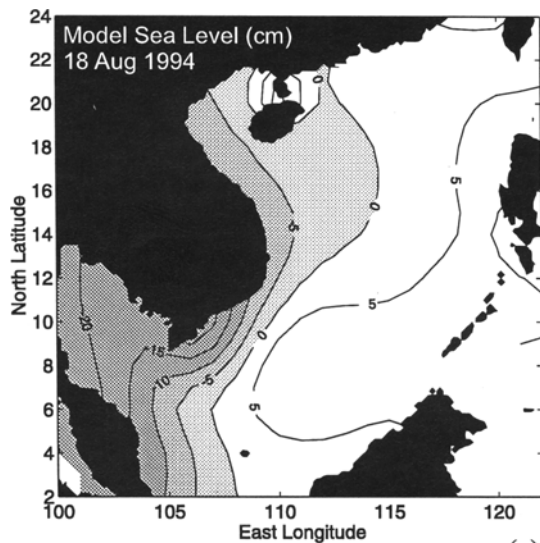
Fig. 4. Sum of the first two sea level modes (a) from model simulated data on Dec. 16, 1992 with a contour interval of 5 cm and (b) from altimeter data on Dec. 12, 1992 with a contour interval of 10 cm. Negative contours are shaded in both plots.

Fig. 5. Same as Fig. 4 but (a) from model simulated data on Dec. 21, 1993 and (b) from altimeter data on Dec. 17, 1993.

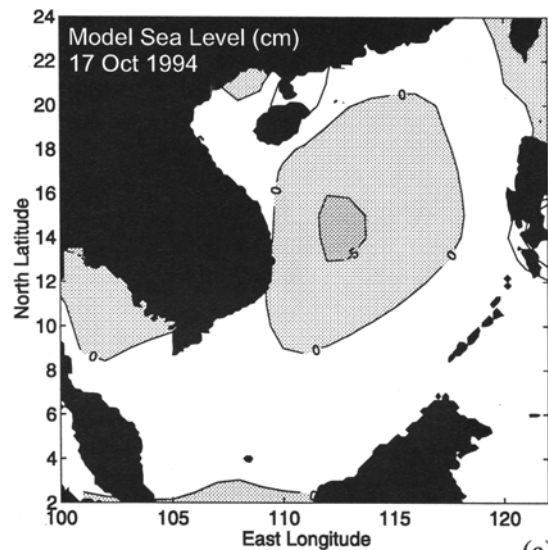
combined with the high off Sunda in mode 1 forms a dipole. The summer pattern persists in the four years, somewhat weaker in July and August of 1993 and 1994, when the mode 2 coefficient is nearly zero. The interannual variation is not clearly shown in the summer sea level field. Further examination of the simulated velocity fields in Section 4 gives a better description of the interannual variations of the summer pattern.

Four snapshots of sea level patterns, two in winter, one in summer, and one during a transition month are obtained from the sum of contributions from the first two sea level modes (Figs. 4–7). These snapshots are chosen to demon-

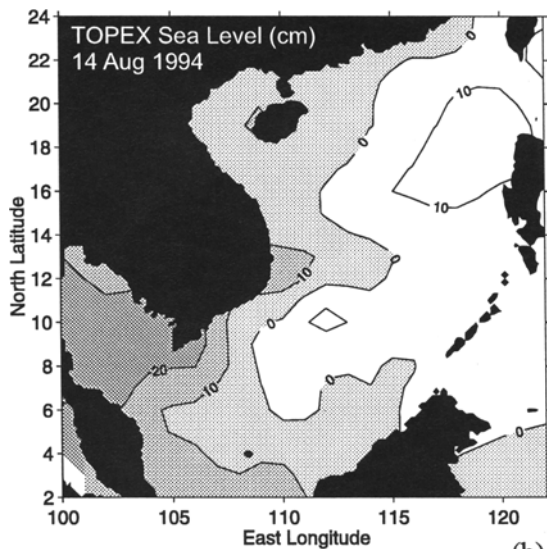
strate seasonal and interannual variations in the sea level field. Similar snapshots are constructed from TOPEX altimeter data in the same time frames from SCF for comparison. Figure 4 shows a weakened sea level field in December 1992. The mode 1 coefficient is large and negative in December (Fig. 3), producing a low in the southern basin. In the meantime, the mode 2 coefficient peaks in November and decreases to nearly zero in December. Without contributions from mode 2, the local minimum in the central basin disappears. A similar pattern exists in the altimeter sea level except in the region west of Luzon, where a low in the altimeter data is missing in the simulated data (Fig. 4(b)).



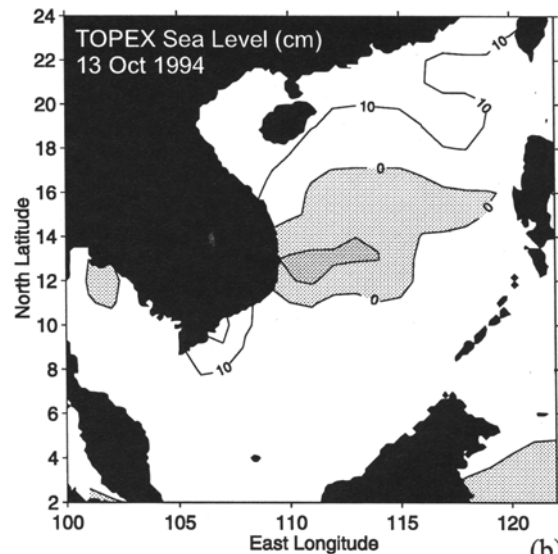
(a)



(a)



(b)



(b)

Fig. 6. Same as Fig. 4 but (a) from simulated data on August 18, 1994 and (b) from altimeter data on Aug. 14, 1994.

Fig. 7. Same as Fig. 4 but (a) from simulated data on Oct. 17, 1994, and (b) from altimeter data on Oct. 13, 1994.

The sea level field in December of the following year corresponds to a strong circulation (Fig. 5). Both mode 1 and mode 2 coefficients are large and negative (Fig. 3). Besides a Sunda low, mode 2 sea level produces a low off Vietnam, resulting in a low spanning the entire central and southern basin. A larger area of low sea level is also shown in the altimeter data.

In August 1994, the sea level is dominated mainly by mode 1 (Fig. 3), which produces a high in the southern basin (Fig. 6(a)). This summer pattern corresponds to that of climatological circulation and is grossly similar to the altimeter sea level field except the high near the Luzon Strait (Fig. 6(b)). As mentioned earlier, year-to-year variations in the summer pattern are not well resolved in the model, and the comparison in other years is not shown. Nevertheless, year-to-year variations do exist in the velocity field and will be discussed in the next section. During the transition month of October 1994, the mode 1 coefficient is small and the mode 2 pattern dominates. A low off Vietnam is present in both the simulated and observed sea level patterns (Fig. 7).

The comparison indicates that our simulation generally captures most features in the basin except two discrepancies. The first is near the Luzon Strait, where a low west of Luzon is not shown in the model sea level. The discrepancy may be due to uncertainties in boundary conditions. Since Wyrski's (1961) transport through the Luzon Strait is specified instead of sea level, the velocity field may give a better description. Another discrepancy is the smaller range of sea level variations in the simulated data. The resolution of the wind field is obtained from interpolation to a 2.5° grid using objective analysis. It is likely that poor wind observations in the South China Sea reduce both the maximum wind speeds and the spatial variability of winds. Nonetheless, the two-gyre pattern is clearly shown in the modes of both simulated and observed data.

4. Horizontal Velocity Modes

The first three EOF modes of horizontal velocities at 50 m depth explain 77%, 10%, and 7% of the total variance, respectively. The spatial distributions of modes 1 and 2 are shown in Fig. 8. Note that in solving the eigenvalue problem, column vectors in e are normalized to unit length (Section 2) and are of magnitude around 0.1 (see Figs. 9 and 10). A maximum vector of 3 m/s in Fig. 8 would give a velocity of about 0.3 m/s, which is about the observed strength. The main feature of mode 1 is a strong boundary current on the Sunda Shelf and southeast of Vietnam. Some water turns eastward between 10° and 14°N , forming a gyre in the southern basin. A weak current continues northward along the coast of Vietnam to the coast of China. In mode 2, the boundary current north of 10°N , flows northward along the shelf edge of northern Vietnam and southern China, forming a gyre off Vietnam. The locations of the two gyres in the first two velocity modes correspond well to the aforementioned

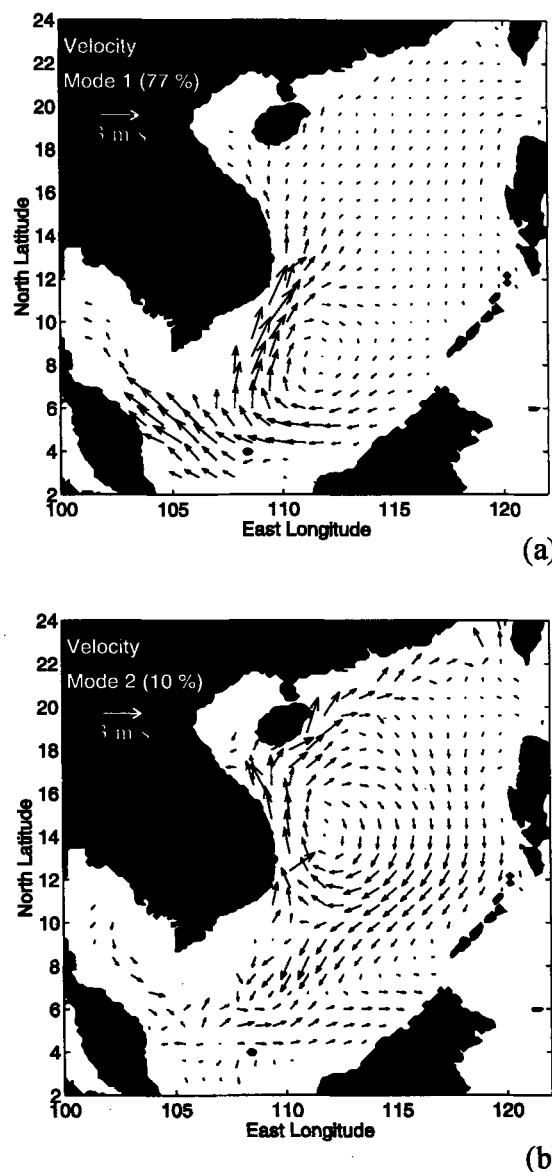


Fig. 8. Spatial structures of the first two horizontal velocity modes at 50 m depth. The scale vector is 3 m/s.

regions of large sea level variations.

Amplitude and phase of the mode 1 coefficient are shown in Fig. 9. Multiplying the amplitude by the magnitude of the current vectors in Fig. 8 gives the speed or the current, while rotating the vectors by the phase angle gives the direction of the velocity. The local extreme values of mode 1 in August and between December and January correspond to the climatological summer and winter gyres during the southwest and northeast monsoons. The local minima in magnitude are in April and October, representing weak mode 1 circulation during the transition months. From November to March, the mode 1 phase is nearly -180° ,

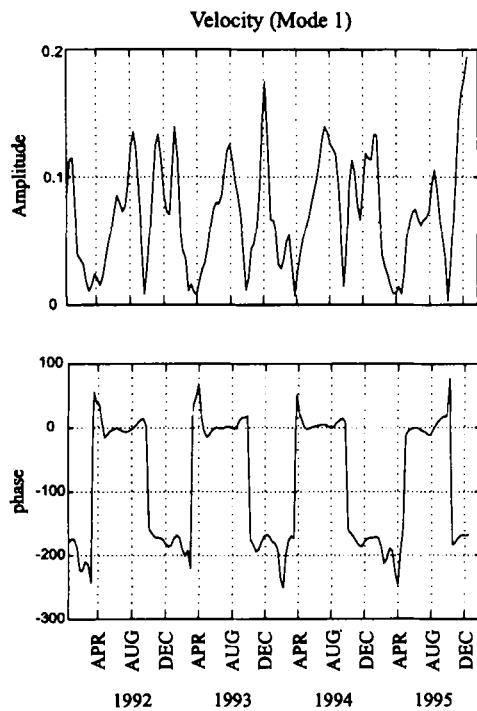


Fig. 9. Amplitude and phase of mode 1 velocity. Time marks indicate the 15th day of each month.

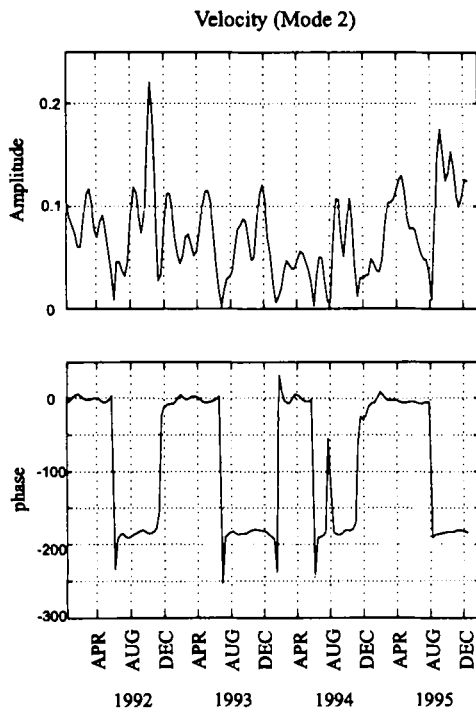


Fig. 10. Same as Fig. 8 but for mode 2 velocity.

indicating a cyclonic gyre in the southern basin. From May to September the phase is close to zero, and the gyre is anticyclonic. The distinct phase change indicates sharp transitions between the winter cyclonic gyre and the summer anticyclonic gyre. Mode 1 alone reveals the annual cycle in the climatological circulation patterns especially in the southern basin. Interannual variations associated with mode 1 are small. The mode 2 coefficient shows phase jumps between 0° to -180° annually as that of mode 1, but the timing is less regular (Fig. 10). In April, the mode 1 coefficient is small, and the velocity field is dominated by mode 2 with a phase of 0° . An anticyclonic gyre appears at about 14° N, 112° E, coinciding with the location of the high off Vietnam in the sea level field. In October, the phase is -180° , and a cyclonic gyre dominates the circulation off Vietnam.

The appearance of a cyclonic gyre off Vietnam in October corresponds to the onset of the northeast monsoon in the northern basin. After October, the phase of the mode 1 coefficient is -180° , and the gyre off Sunda Shelf also becomes cyclonic. The two gyres off Vietnam and Sunda Shelf overlap, as demonstrated in the circulation pattern obtained from the sum of the two modes on December 1, 1993 (Fig. 11(a)). A southward boundary current extends from China to the Sunda Shelf. This pattern agrees with the picture of a basin-wide cyclonic gyre in Wyrski's (1961) atlases. The winter gyre is maintained until a change in phase of the mode 2 coefficient in late winter. The cyclonic circulation in the northern basin becomes anticyclonic, resulting in a weakened basin-wide gyre. In the winter of 1993–1994, such a transition does not occur until February, 1994 (Fig. 10), and the basin gyre is maintained through that winter. On the other hand, the mode 2 coefficient changes sign in late November in 1992 and 1994, too early for a basin-wide cyclonic gyre to develop. The situation is demonstrated in the circulation pattern on December 6, 1992 (Fig. 11(b)). The cyclonic circulation and the coastal current exist only in the southern basin, south of 12° N.

After February, the mode 1 coefficient is small, and the winter gyre off Sunda Shelf diminishes. In spring, the mode 2 coefficient is 0° in all years (Fig. 10), and the circulation is dominated by an anticyclone off central Vietnam. After April a mode 1 anticyclone begins to develop off Sunda Shelf. Climatological atlases (Wyrski, 1961) consistently show development of an anticyclonic gyre in the northern basin in April and May and receding of the gyre to the southern basin from May to August. Transition from an anticyclonic northern gyre to a cyclonic gyre begins in summer, but its timing varies from year to year: June in 1992 and 1994, July in 1993 and August in 1995. After the transition, the northern cyclone and the southern anticyclone form a dipole structure with an eastward jet. The circulation patterns before and after the transition are shown in the flow fields on July 23, 1995 and August 29, 1992,

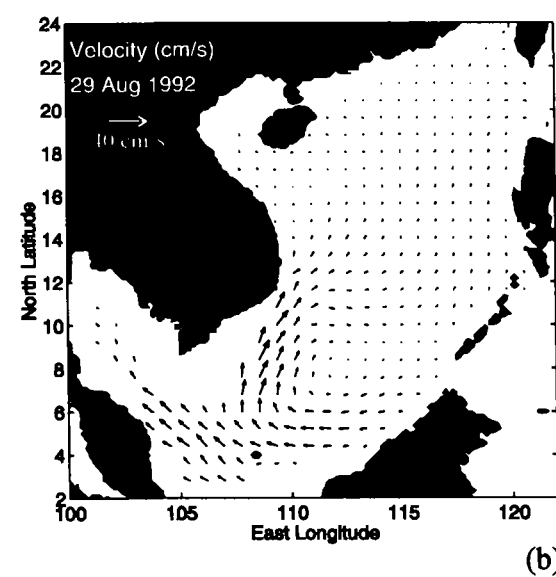
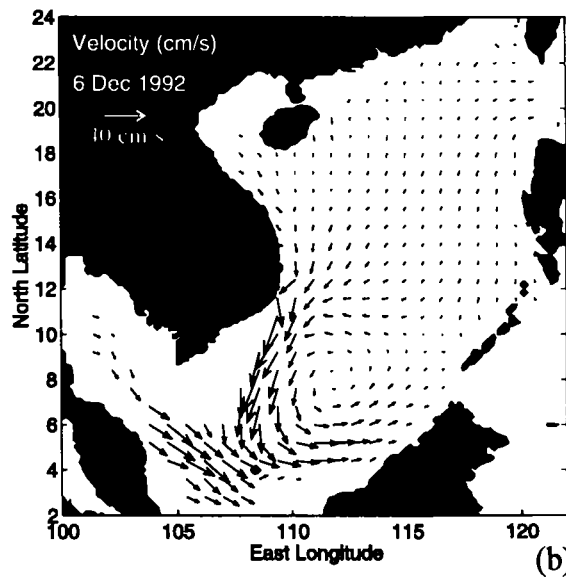
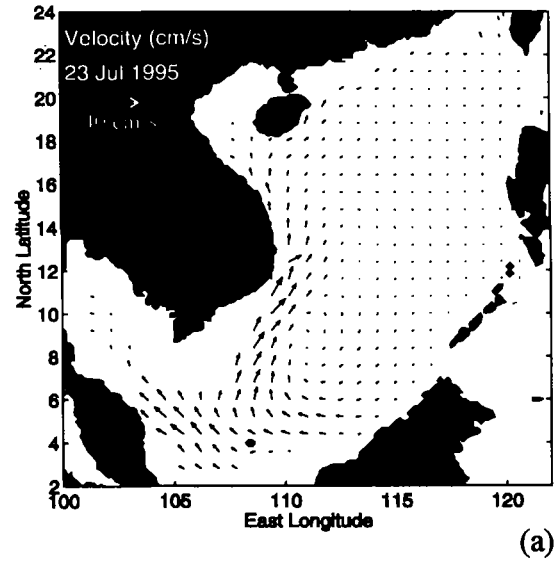
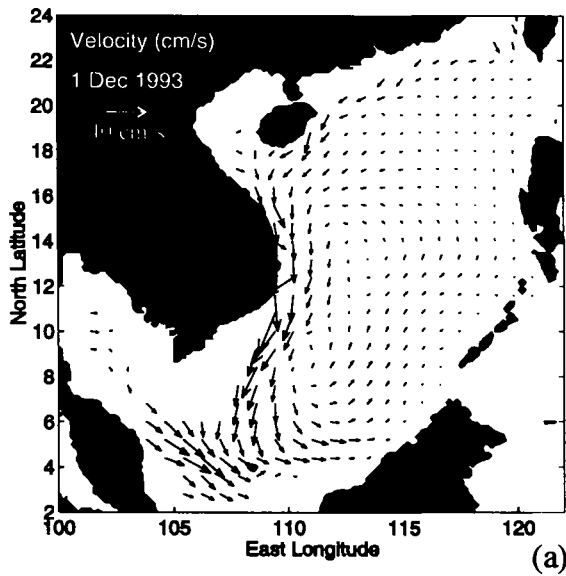


Fig. 11. Sum of the first two horizontal velocity modes on (a) Dec. 1, 1993 and (b) Dec. 6, 1992. The velocity scale is 40 cm/s.

Fig. 12. Same as Fig. 10 but on (a) Jul. 23, 1995 and (b) Aug. 29, 1992.

respectively (Fig. 12). In 1995, a late transition of the northern gyre from anticyclonic to cyclonic allows a northward coastal jet to penetrate into the Gulf Tonkin. In contrast, an eastward jet leaves the coast of Vietnam on August 29, 1992 as in the climatological summer circulation pattern described by Wyrтки (1961).

5. Vertical Velocity Modes

The first three vertical velocity modes explain 70%, 16%, and 6% of the total variance, respectively. The spatial distribution of mode 1 shows out-of-phase variations in the southeast and northwest parts of the basin (Fig. 13(a)). Local

maxima are located off Borneo and off southeast Vietnam. The locations of large vertical velocity are consistent with areas of upwelling in the South China Sea except northwest of Luzon (Shaw *et al.*, 1996). Again, this discrepancy is likely due to uncertainties in the boundary conditions at the Luzon Strait in the model. The mode 2 variation is mainly in a region extending eastward from the coast of Vietnam, but the magnitude is much smaller than that in mode 1 (Fig. 13(b)). Since the normalization is based on temporal variations, the spatial variation indicates that the mode 2 vertical velocity field is generally small compared to mode 1. This statement is verified by comparing the vertical

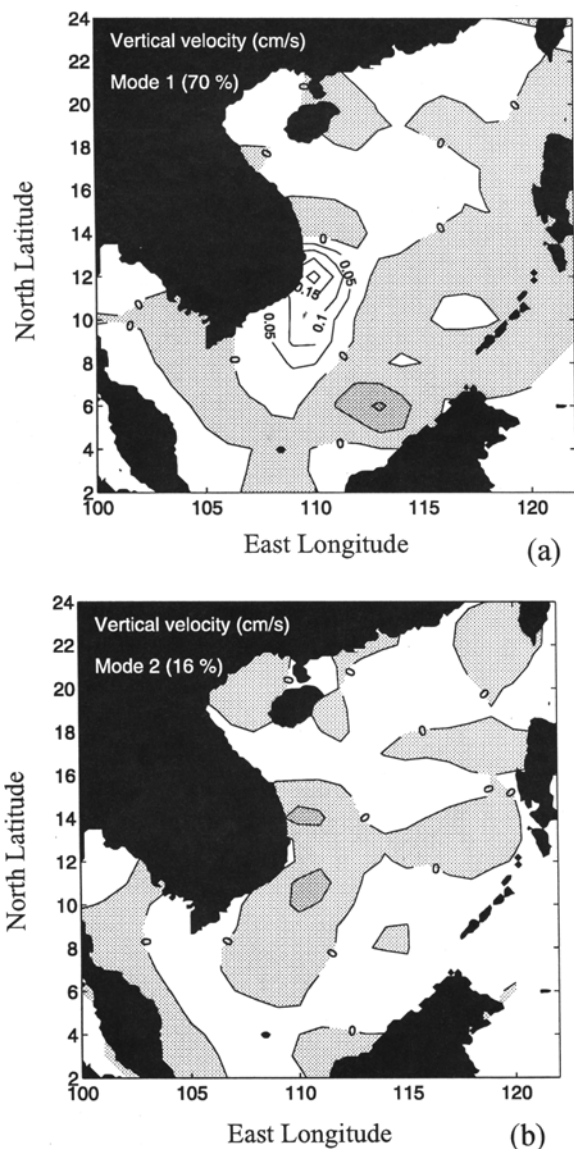


Fig. 13. Spatial structure of the first two vertical velocity modes. Contour intervals are 0.05 cm/s, and negative contours are shaded.

velocity fields contributed by the first few modes. It is found that the mode 1 variation captures most qualitative features in the simulated fields. Therefore, only the first mode is discussed below.

The mode 1 temporal variation is shown in Fig. 14. The variation is similar to that of mode 1 sea level. The coefficient is positive in summer and negative in winter, close to zero in April and October. A positive coefficient appears from May to August, showing upwelling centered at 12°N off the coast of Vietnam and downwelling off Borneo. Summer upwelling off Vietnam has been reported in both observations (Wyrki, 1961) and model simulation (Chao *et al.*,

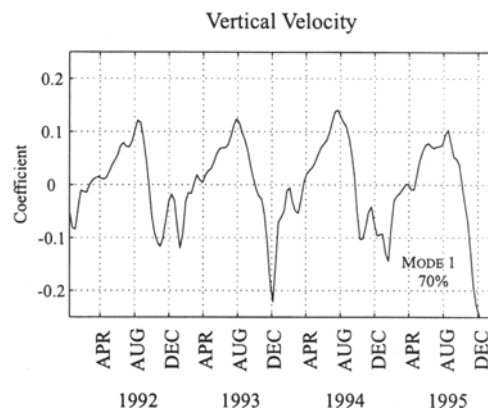


Fig. 14. Same as Fig. 3 but for the first vertical velocity mode.

1996a). A negative coefficient is present from October to March, indicating downwelling off Vietnam and upwelling off Borneo. Winter upwelling at the edge of Sunda Shelf is a prominent feature in the South China Sea (Wyrki, 1961). Upwelling and downwelling in winter show significant interannual variations. The negative peak is strong and narrow in December 1993 and 1995, but weak and broad from October to February in 1992 and 1994. Thus, winter downwelling off Vietnam is weaker in 1992 and 1994 than in 1993 and 1995, consistent with a weaker basinwide winter gyre in December 1992 and 1994 (Section 4). A weaker vertical velocity field associated with a weaker winter gyre has been inferred in the numerical simulation of Chao *et al.* (1996b).

6. Wind Stress Curl Modes

The modeling efforts in recent years (Pohlmann, 1987; Shaw and Chao, 1994; Chao *et al.*, 1996b) have collectively revealed that the circulation of the South China Sea is dominated by local wind forcing. Intuitively, it is not clear whether the wind stress or its curl is more important. Several simulations by the authors using Princeton Ocean Model on a β -plane were carried out in order to investigate which factor dominates the formation of a gyre (not shown). The results show that there is no gyre if there is no wind stress curl. The formation of a gyre, whatever anticyclonic or cyclonic, is essentially determined by the wind stress curl. Wind stress curl forcing is consistent with the basic Stommel model (1948). SCF also found that the first two modes of the wind stress curl agree well with those in the corresponding altimeter sea level modes, further supporting the wind stress curl forcing scenario.

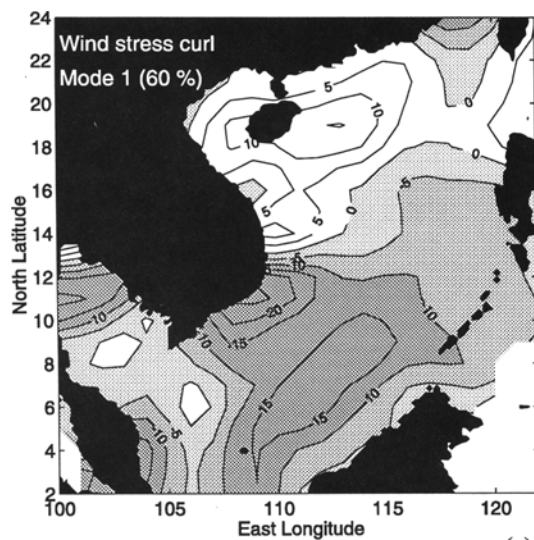
In this section, wind stress curls are calculated from the wind stress field used to drive the model and are decomposed into EOF modes as the sea level and velocity fields. The first three EOF modes explain 60%, 22% and 4% of the total variance respectively. Thus, the first two modes could reveal information on how sea level and velocity fields are

driven. Modes 1 and 2 bear resemblance to the corresponding simulated sea level and horizontal velocity fields (Fig. 15). Mode 1 consists of negative values in the deep basin, extending from the Sunda Shelf to Luzon with a local minimum in the southern basin. Large positive values are in the northwest basin. Mode 2 consists of negative values off Vietnam with a local minimum centered at 14°N. The locations of the two minima in the first two modes correspond well to aforementioned regions of large sea level variations and gyres in the horizontal velocity modes.

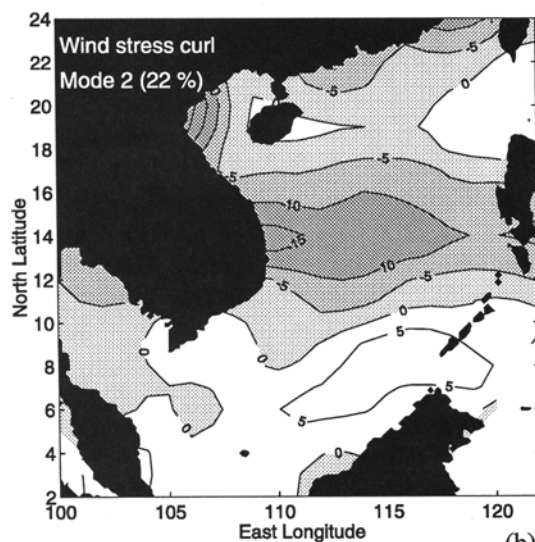
Temporal variations of the first two modes of the wind stress curl (Fig. 16) agree with those in the corresponding

simulated sea level and velocity fields. The extreme positive and negative coefficients of mode 1 show peak negative and positive curls in the southern basin in August and December, respectively. The extreme wind stress curls coincide with climatological anticyclonic and cyclonic southern gyres (Fig. 11). Mode 2 modifies the climatological circulation and shows interannual variations. The mode 2 coefficient remains negative from October through the end of December in 1993 and 1995 but becomes either positive in December 1992 or near zero in December 1994. A negative coefficient enhances the positive curl in the central basin and thus strengthens the winter gyre. This is indeed the case in late 1993 and 1995. On the other hand, a positive coefficient would weaken the gyre in the central basin as in late 1992 and 1994 (Section 4).

In April, the mode 1 contribution is small (Fig. 16). Increase in amplitude of mode 1 coefficient from May to August provides negative curls to the southern basin and produces an anticyclonic gyre there. In the meantime, the mode 2 coefficient rapidly becomes negative into summer and produces a positive curl and a cyclonic northern gyre. The southern and northern gyres form the climatological dipole structure shown in earlier studies (Shaw and Chao, 1994). In summer 1993 and summer 1995, the mode 2 coefficient remains positive until August, and development of the climatological dipole system is delayed. A weaker central gyre in summer in these two years are also noted in Section 4.



(a)



(b)

Fig. 15. Spatial structure of the first two wind stress curl modes. Contour intervals are $5 \times 10^{-7} \text{ Nm}^{-3}$, and negative contours are shaded.

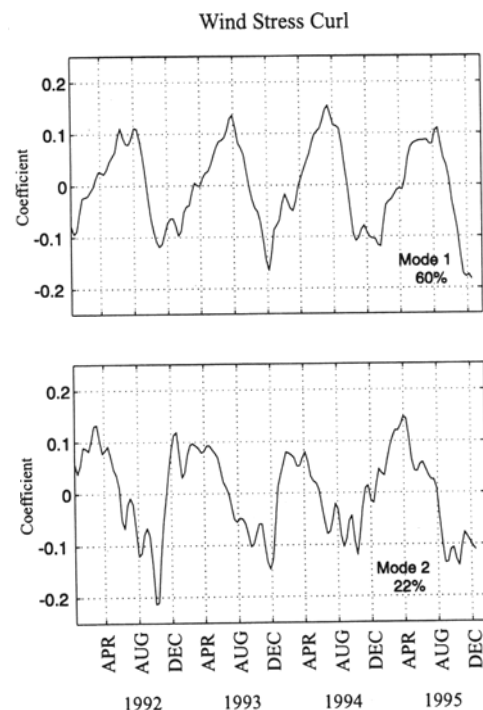


Fig. 16. Same as Fig. 3 but for the first two wind stress curl modes.

7. Discussion

Warming episodes in the tropical Pacific occurred in 1991–1992, 1993 and 1994 (Goddard and Graham, 1997). The episode in 1991–1992 peaked in May 1992, and by October 1992, all atmospheric and oceanic indices were indicating a return to normal conditions. However, patches of weak, warm anomalies in sea surface temperature still lingered on and excited a weak warming in early 1993. Conditions returned to nearly normal by late 1993. Another warming event started in the summer of 1994 and followed by the La Niña episode of 1995–1996. Thus, the normal summer circulation is expected in 1992 following the 1991–1992 warm event. The climatological circulation may also prevail in the winter of 1993–1994 and summer 1994 during a long break in warming. A strong gyre in the winter of 1995–1996 should appear during the La Niña episode. Otherwise, the South China Sea circulation should be in a weakened state.

Lack of a basin-wide cyclonic winter gyre in late 1992 and 1994 can be largely explained by the reversal of a northern gyre in early December. The reversal, due to a diminishing northeast monsoon, weakens the cyclonic circulation in the northern basin. In the simulation of the 1982–1983 El Niño episode, Chao *et al.* (1996b) show weakening of the winter gyre in late 1982 under a weak monsoon and strengthening of a cyclonic winter gyre in fall 1983 under a record-strength northeast monsoon. In the altimeter sea level field, SCF found similar weakening of the winter gyre in late 1992 and late 1994 and strengthening of a basin-wide cyclonic gyre in the winter of 1993–1994. The reversal of the northern gyre in early summer also affects the summer circulation pattern. Because of early reversals, summer circulation is stronger in 1992 and 1994 than in 1993 and 1995. The study of SCF also shows a strong summer circulation pattern with a dipole and a jet in 1994. Thus, the weakened South China Sea circulation from late 1992 to mid-1993 and from late 1994 to mid-1995 grossly coincides with the warm episodes in the tropical Pacific.

The reversal of two gyres in the simulated velocity modes can also be seen in the sea level modes. The mode 2 sea level off Vietnam is high in spring and low in fall, corresponding well to the northern gyre in the mode 2 velocity field. The change in signs of the sea level coefficient in December in 1992 and 1994, agrees with early reversal of the northern gyre, resulting in a weak winter gyre. The early transition from a high to a low in June 1992 is also present in the sea level modes. However, the dipole structure is shown to a lesser extent in the simulated sea level field than in either the altimeter data or the simulated velocity field. As mentioned in Section 3, improving the boundary specification in the Luzon Strait and wind observations is likely to provide a better description of the circulation in the South China Sea.

The simulated sea level and horizontal velocity fields

follow variations in the wind stress curl. The mode 1 sea level and horizontal velocities correspond to a symmetric reversal of the winter and summer gyres and is consistent with changes in the mode 1 wind stress curl. The mode 2 variation in the wind stress curl contributes to the asymmetry in the winter and summer gyres with interannual variations. In winter, a cyclonic gyre spanning the central and southern basin and a southward western boundary current form when both modes contribute positive wind stress curls. When the mode 2 contribution is weak or of opposite sign, the winter gyre is confined in the southern basin. A weak winter gyre appears during the El Niño years in late 1992 and late 1994. In summer, contributions of positive curls from mode 2 in the central basin and negative curls in the southern basin produce the dipole structure with a northward coastal current leaving the coast of central Vietnam. Weakening of the mode 2 wind stress curl in summer prevents the formation of such a coastal jet in 1993 and 1995. Weakened circulation and a lower rate of upwelling under weakened monsoon winds in the South China Sea during El Niño events in 1992–1995 are generally consistent with the conclusion derived from simulation in 1982–1984 by Chao *et al.* (1996b).

8. Summary and Conclusions

The seasonal and interannual variations of the South China Sea circulation can be described in two velocity modes. The first mode describes the reversal of a southern gyre in April and October. The reversal, cyclonic in winter and anticyclonic in summer, shows little year-to-year variation. On the other hand, the mode 2 variation, associated with a northern gyre off Vietnam, shows significant interannual variations. In normal years, a cyclonic northern gyre persists from summer well into January. After the development of a cyclonic southern gyre in October, the cyclonic circulation expands over the entire basin as observed in the climatological circulation pattern (Wyrtki, 1961). Reversal of the northern gyre in late fall, due to a weakening northeast monsoon, weakens the circulation in the north. The winter gyre seems to be confined in the southern basin. The northern anticyclone becomes cyclonic in early summer and forms a dipole with the anticyclonic southern gyre developed in late spring. This dipole structure and its associated eastward jet leaving the coast of Vietnam are well described in the climatological circulation (Shaw and Chao, 1994). A late transition from an anticyclonic northern gyre to a cyclone prevents the formation of the summer dipole system. Vertical motions are weaker during weaker basin-wide circulations.

Modulation of the circulation by El Niño is clearly shown in the simulation. Two episodes of weaker circulation patterns in the South China Sea during 1992–1995 are identified: from late 1992 to mid-1993 and from late 1994 to mid-1995. In late 1992 and 1994, a basin-wide cyclonic

winter gyre did not develop. A northern cyclone, which normally appears in June each summer, did not develop in 1993 and 1995 until after July, preventing the formation of a dipole. The episodes correspond well to the El Niño events of 1992–1995 in the Equatorial Pacific.

Wind stress curl forcing seems to be the dominant process controlling the circulation in the South China Sea. Contribution from the wind stress curl is mostly from the first two empirical orthogonal modes. Wind stress curl forcing in the southern basin is mainly contributed by mode 1; its sign change produces symmetrical cyclonic and anti-cyclonic gyres in winter and summer, respectively. Wind stress curl forcing in the central basin is mostly due to mode 2 variation. Contribution from this mode produces the asymmetry in winter and summer, a cyclonic winter gyre spanning the whole basin and a dipole structure in summer. During El Niño years, mode 2 contribution of the wind stress curl is not important, and the circulation of the South China Sea is weakened. The agreement between variations of the wind stress curl and the velocity field suggests that the wind stress curl is the dominant driving force of the circulation in the South China Sea.

Acknowledgements

This manuscript is greatly improved by suggestions of the reviewers. This research was supported by the U.S. National Science Foundation under grants OCE95-02984 (PTS) and OCE95-04959 (SYC). The North Carolina Supercomputing Center provided CPU time on its Cray T90 for the model simulation. This is UMCES contribution 3078.

References

- Chao, S.-Y., P.-T. Shaw and S. Wu (1996a): Deep water ventilation in the South China Sea. *Deep-Sea Res.* **1**, 43, 445–466.
- Chao, S.-Y., P.-T. Shaw and S. Wu (1996b): El Niño modulation of the South China Sea circulation. *Progress in Oceanography*, **38**, 51–93.
- Csanady, G. T. (1982): *Circulation in the Coastal Ocean*. Reidel, Dordrecht, Holland, 279 pp.
- Goddard, L. and N. E. Graham (1997): El Niño in the 1990s. *J. Geophys. Res.*, **102**, 10423–10436.
- Kalnay, E., M. Kanamitsu, R. Kistler, W. Collins, D. Deaven, L. Gandin, M. Iredell, S. Saha, G. White, J. Woollen, Y. Zhu, M. Chelliah, W. Ebisuzaki, W. Higgins, J. Janowiak, K. C. Mo, C. Ropelewski, J. Wang, A. Leetmaa, R. Reynolds, Roy Jenne and D. Joseph (1996): The NCEP/NCAR 40-year reanalysis project. *Bulletin of the American Meteorological Society*, **77**, 437–471.
- Levitus, S. (1982): Climatological atlas of the world ocean. NOAA Professional paper No. 13, U.S. Government Printing Office, Washington, D.C., 173 pp.
- Levitus, S. (1984): Annual cycle of temperature and heat storage in the world ocean. *J. Phys. Oceanogr.*, **14**, 727–746.
- Nitani H. (1972): Beginning of the Kuroshio. p. 129–163. In *Kuroshio*, ed. by H. Stommel and K. Yoshida, University of Washington Press, Seattle.
- Pohlmann, T. (1987): A three-dimensional circulation model of the South China Sea. p. 245–268. In *Three-Dimensional Models of Marine and Estuarine Dynamics*, ed. by J. J. Nihoul and B. M. Jamart, Elsevier, New York.
- Shaw, P.-T. and S.-Y. Chao (1994): Surface circulation in the South China Sea. *Deep-Sea Res.*, **41**, 1663–1683.
- Shaw, P.-T., S.-Y. Chao, K.-K. Liu, S.-C. Pai and C.-T. Liu (1996): Winter upwelling off Luzon in the northeastern South China Sea. *J. Geophys. Res.*, **101**, 16435–16448.
- Shaw, P.-T., S.-Y. Chao and L.-L. Fu (1997): Sea surface height variations in the South China Sea from satellite altimetry (submitted to *Oceanographica Acta*).
- Stommel, H. M. (1948): The westward intensification of wind-driven ocean currents. *Transactions American Geophysical Union*, **29**, 202–206.
- Trenberth, K. E. and T. J. Hoar (1996): The 1990–1995 El Niño—Southern oscillation event: longest on record. *Geophys. Res. Lett.*, **23**, 57–60.
- Wyrski, K. (1961) Physical oceanography of the southeast Asian waters. NAGA Report Vol. 2, Scientific Results of Marine Investigation of the South China Sea and the Gulf of Thailand, Scripps Institution of Oceanography, La Jolla, California, 195 pp.